Transactions of the Korean Nuclear Society Spring Meeting
Jeju, Korea, May 9-10, 2024

Evaluation of mechanical properties and helium swelling response of Ti/Ta-RAFM steels under Fe ion irradiation and helium implantation

Sangeun Kim [a,b], Jinwoo Park [a], Hyung-Ha Jin[b], Chang-Hoon Lee [c], *Chansun Shin [a],
[a] *Department of Materials Science and Engineering, Myongji University*
[b] *Nuclear Materials Safety Research Division, Korea Atomic Energy Research Institute(KAERI)*
[c] *Ferrous Alloy Department, Korea Institute of Materials Science (KIMS)*
[*] *Corresponding author: c.shin@mju.ac.kr*

1. Introduction

In a fusion reaction, about 80% of the energy is emitted as 14.1 MeV neutrons. The 14.1 MeV neutrons decay to ~0.025 eV through elastic and inelastic processes and have a broad neutron energy spectrum, producing atomic displacements and nuclear transmutation gases (H, He) [1]. This causes irradiation hardening, swelling by helium bubbles, and hydrogen embrittlement, which leads to structural problems and changes in mechanical properties of the material.
Reduced Activation Ferritic/Martensitic (RAFM) steel is one of the candidate structural materials for fusion reactor blankets. It is similar to the 9Cr-1Mo-based material used in thermal power plants and was developed by replacing the high-activity elements Mo, Nb, and Ni with the low-activity elements W, V, and Ta [2].
The purpose of this study is to evaluate irradiation hardening and helium bubble swelling by heavy ion irradiation and helium implantation on a developed Ti/Ta-RAFM (10Ta1Ti-T700 and 10Ta1Ti-T730) steel and a reference steel (similarly Eurofer97), respectively.

2. Experimental

Irradiation conditions were 6MeV-Fe^{2+}ion and irradiation dose of 1×10^{16} ions/cm^2. It was carried out at room temperature. The calculated peak damage and Fe ion concentration is 10 dpa at a depth of 1.4 μm and 2500 appm at 1.7 μm, respectively. **[Fig. 1]** FIB (Focused Ion Beam) was utilized to fabricate micropillars with a diameter of approximately 500 nm and perform compression tests **[Fig. 2]**.
A Cu TEM grid with a mesh structure of $35\times35\mu m^2$ hole size was attached to the surface of polished specimen to compare the effects of implanted and unimplanted regions. 160keV He ions were implanted into the RAFM steels with the dose of 0.5×10^{17} ion/cm2 and 1.0×10^{17} ion/cm^2 in a vacuum chamber at room temperature. He ion concentrations are 1.2dpa, 2.4 dpa at 450 nm depth and 3%, 6% at 500 nm, respectively **[Fig. 1]**. The TEM grid was detached from the specimen and then PIA (post-implantation annealing) at 300 - 500℃ for 2hours. After PIA, the surface height of the specimen was measured by 3D surface profiler **[Fig. 3(a)]**. Nanoindentation mapping was performed using a nanoindenter to confirm the difference in nanohardness between the helium implanted area and the unimplanted area **[Fig. 3(b)]**.
SEM and TEM were utilized to analyze dislocation loop and helium bubbles, and more.

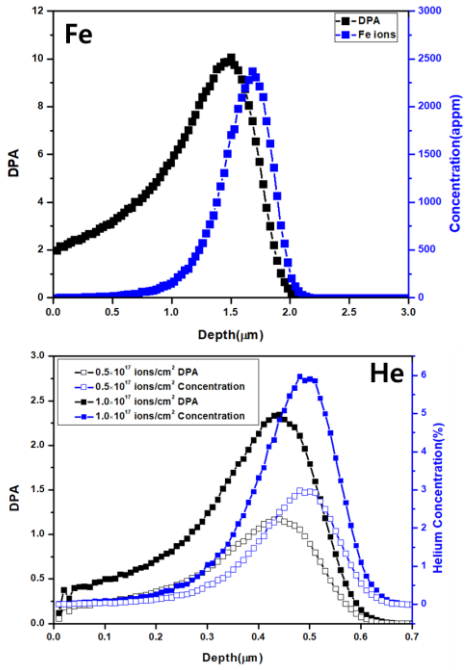

Fig. 1. Depth-dependent dose and implanted ion concentration profiles for Fe/He ion calculated with the SRIM code

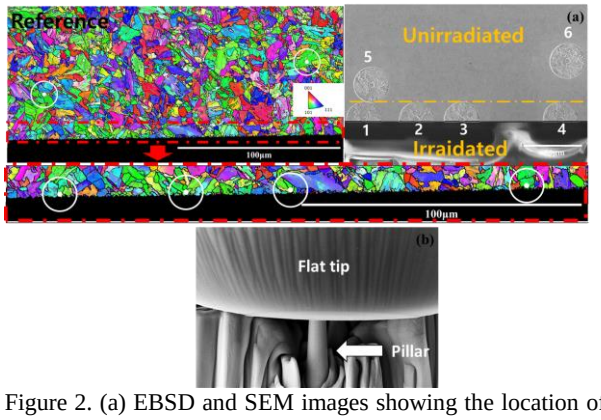

Figure 2. (a) EBSD and SEM images showing the location of the micropillars fabricated in the plane perpendicular to the irradiation plane. The large circle is the outer circle of approximately 30 um and the center dot is the 500 nm micropillars. (b) In-situ micropillar compression test SEM image.

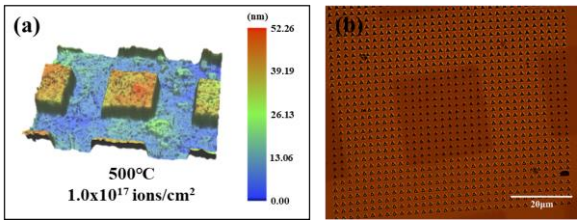

Figure 3. (a) Surface step and (b) nanoindentation mapping images of the specimen after helium implantation and PIA.

3. Result and Discussion

Fig. 4 shows the SEM images of the micropillars before and after the micro-compression test. The deformed morphologies of unirradiated micropillars shows pronounced slip steps and slip traces along the offsets on parallel plane, as pointed out by arrow in **Fig. 4(b)**. Successive slip steps occur as dislocations escape to the free surface [3]. The dislocation stops near the surface before escaping. The irradiated micropillars show less pronounced slip steps and wide slip bands compared to unirradiated micropillars, as indicated in brackets **[Fig. 4(c)]**. Radiation defects formed by irradiation with Fe ions act like nano-scale particles, preventing dislocations from escaping to the surface. Thus, the deformation is caused by slip bands, not pronounced slip steps.

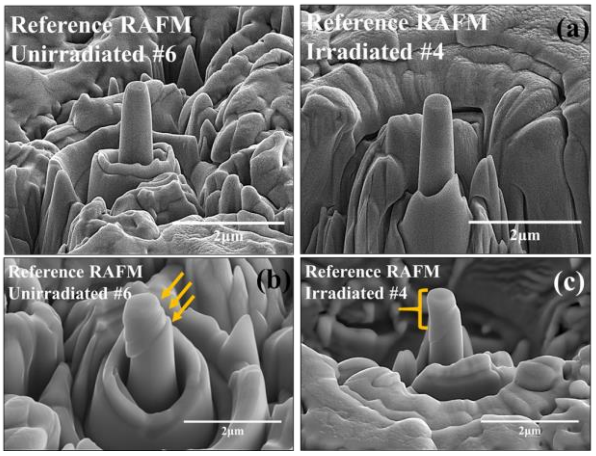

Figure 4. SEM images of 500 nm unirradiated and irradiated micropillars of reference RAFM steel, (a) before and (b), (c) after compression (yellow arrow indicates a slip shape).

The change in yield strength according to the change in test specimen size is shown in the **[Fig. 5]**. Size effects in unirradiated materials are related to the interaction of microstructural features (such as grain boundaries) and dislocations. The size of the specimen at the point where the two zones (“smaller is weaker/stronger”) transition depends on microstructure feature and grain size differences.

Size effects are not known to occur in irradiated materials. The nanoscale radiation-induced defects formed by irradiation create new small length scales inside the material. Radiation-induced defects control the decrease or increase in yield strength due to size effects through interaction with dislocations, and size-independent strength is measured even at smaller sizes compared to unirradiated materials. The bulk yield strength of Ti/Ta - (T700, T730), a reference steel, was measured by tensile testing. Comparing this to the yield strength of the micropillar test in the unirradiated area, it was confirmed that the yield strength is lower at the bulk size. It is assumed to follow the "smaller is stronger" trend in **[Fig. 5]**.

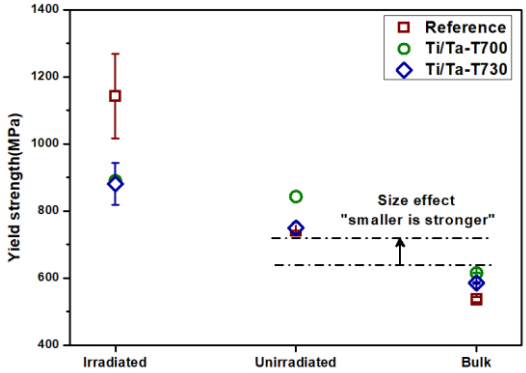

Figure 5. Yield strengths evaluated in 500 nm irradiated and unirradiated Ti/Ta-RAFM and reference RAFM steels are shown, as well as the yield strength of the bulk material obtained by tensile testing. The variation of yield strength with specimen size for unirradiated material is shown by dotted lines and arrows.

Fig. 6 shows a 3D image obtained by measuring the surface change of T700 RAFM steel using a 3D surface profiler. Areas injected with helium through the TEM grid holes show distinct surface differences from non-injected areas due to swelling. **Fig. 7** shows the average of the surface step for each condition and specimen. T700 and reference steel show similar trends overall, with T730 showing the best resistance to helium bubble swelling. It can be seen that the surface step increases with increasing helium-injection amount and PIA temperature. At 300℃ and 400℃, the surface step shows a similar trend. And at 500℃, the surface step increases dramatically.

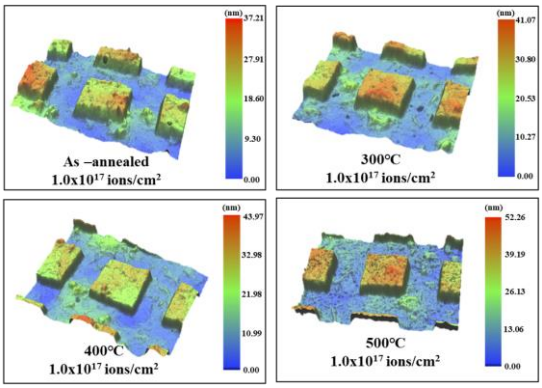

Figure 6. Ti/Ta-T700 sample with 3D surface profiler observing the change in surface step with PIA temperature after helium implantation.

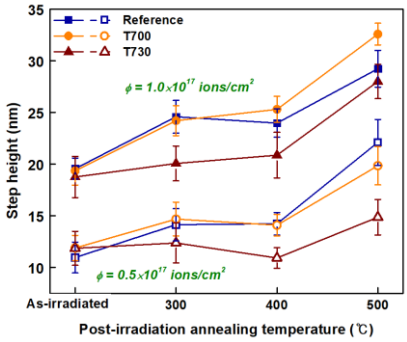

Figure 7. Variation of surface step height as a function of helium implantation concentration and PIA temperature for Ti/Ta-RAFM and Reference steels.

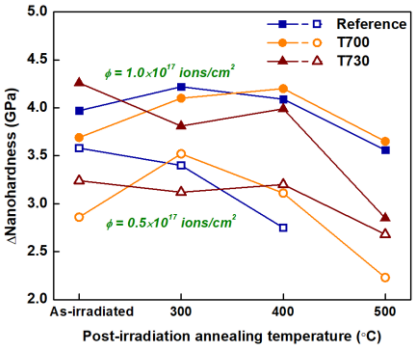

Figure 8. Mapping results as a function of helium implantation concentration and PIA temperature for Ti/Ta-RAFM and Reference steels. Δnanohardness on the y-axis represents the helium implanted area minus the unimplanted area.

The change in hardness due to helium bubble swelling as a function of PIA temperature and helium-implantation concentration is shown in the **[Fig. 8]**. Unlike the helium swelling surface step measurements, there is no clear trend between the reference steel and Ti/Ta-RAFM steel. As the helium injection volume increased, it was observed that the hardness values were higher. Furthermore, the overall trend is similar up to PIA temperature 400℃, but a drastic decrease in delta hardness was observed at 500℃.

At low temperatures (300℃ > T), the effect is due to small clusters, and 300-400℃ is the nucleation region of helium bubbles, where the hardening seems to be caused by small helium bubbles. The drastic decrease in hardness at 500°C is associated with either recovery or helium bubble growth [4, 5]. However, the increase in surface step even at 500℃ suggests that the decrease in hardness is due to helium bubble growth rather than recovery.

For Reference steel and Ti/Ta-RAFM steel, the tempered martensite structure consists of sub-grains (packet, block, lath) within prior-austenite grains (PAGs). SEM images confirm the presence of M23C6, a Cr-rich carbide in the interlath, and MX, a fine precipitate observed within the lath **[Fig. 9]**. Ti/Ta-RAFM steel and reference steel have similar block widths of 0.5-1.0 μm and PAGs sizes of approximately 10 μm [6]. **Fig. 9** shows SEM images for M23C6, MX, and each precipitate fraction utilizing the Image J program. M23C6 precipitate size was smallest for T700 and largest for Reference steel. For T730, the fraction was about twice as high as for the other two steels. For MX precipitates, the fractions were similar for all three steels, with differences in size in the order T700 < T730 < Reference **[Fig. 10]**.

The superior resistance of the development steels, T700 and T730, to irradiation hardening and helium swelling compared to the reference steel was found to be a function of precipitate size and fraction.

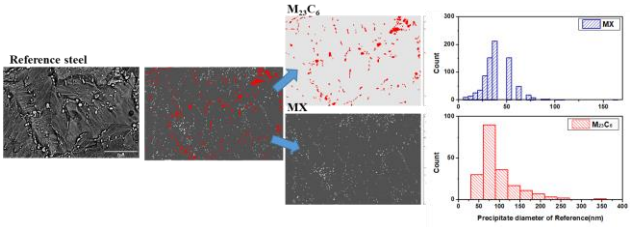

Figure 9. SEM images of reference steel after etching were analyzed with the image j program to quantitatively measure the diameter and fraction of M23C6 and MX precipitates.

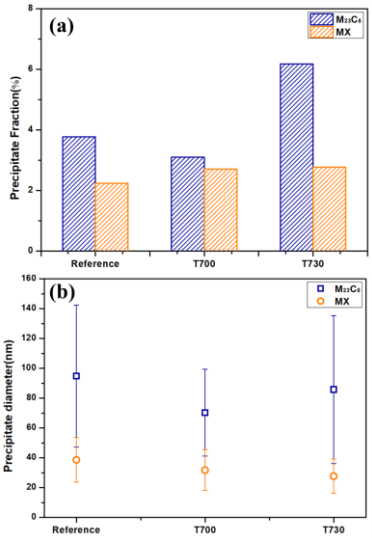

Figure 10. The precipitate (a) fraction and (b) diameter of the reference steel and Ti/Ta-RAFM steel are shown

REFERENCES

[1] Garry McCracken, Peter Stott, Fusion: The Energy of the Universe, Elsevier Inc, 2012.

[2] C. Wang, Q. Cui, X. Huo, C. Zhang, W. Xu, Design of Reduced Activation Ferritic/Martensitic Steels by Multiphase Optimization during the Entire Processing, ISIJ International. 59 (2019) 1715-1722.

[3] W.S. Choi, S. Sandlöbes, N.V. Malyar, C. Kirchlechner, S. Korte-Kerzel, G. Dehm, B.C. De Cooman, D. Raabe, Dislocation interaction and twinning-induced plasticity in face-centered cubic Fe-Mn-C micro-pillars, Acta materialia. 132 (2017) 162-173.

[4] H. Trinkaus, B.N. Singh, Helium accumulation in metals during irradiation – where do we stand?, Journal of nuclear materials. 323 (2003) 229-242.
[5] I. Carvalho, H. Schut, A. Fedorov, N. Luzginova, P. Desgardin, J. Sietsma, Dose effects in He implanted Eurofer97 steel, Journal of physics. Conference series. 505 (2014) 12019-4.
[6] C. Lee, J. Park, W. Seol, J. Moon, T. Lee, N.H. Kang, H.C. Kim, Microstructure and tensile and Charpy impact properties of reduced activation ferritic–martensitic steel with Ti, Fusion engineering and design. 124 (2017) 953-957.